POLITECNICO DI TORINO
Repository ISTITUZIONALE

Suspension electrospinning of SBR latex combined with photo-induced crosslinking: control of nanofiber composition, morphology, and properties

(Article begins on next page)

27 July 2024

Polymers & biopolymers

Suspension electrospinning of SBR latex combined with photo-induced crosslinking: control of nanofiber composition, morphology, and properties

Parnian Kianfar[1,4,*], Ahmed Bakry[2], Sara Dalle Vacche[1,3], Roberta Bongiovanni[1,3], and Alessandra Vitale[1,3,*]

[1] *Department of Applied Science and Technology, Politecnico di Torino, 10129 Turin, Italy*

[2] *Chemistry Department, Helwan University, Cairo 11795, Egypt*

[3] *INSTM – Politecnico di Torino Research Unit, 50121 Florence, Italy*

[4] *Present Address: Department of Materials Science and Engineering, Sharif University of Technology, Tehran, Iran*

ABSTRACT

Suspension electrospinning of a styrene-butadiene rubber (SBR) latex coupled with photo-induced crosslinking in ambient conditions is proposed as a rapid method to prepare ultrafine shape-stable rubber fibrous membranes. Polyethylene oxide (PEO) is used as template polymer and can eventually be removed from the nanostructured membrane by a simple water treatment. A multifunctional thiol crosslinker and an appropriate photo-initiating system are added to the latex to allow the fast and efficient photo-induced crosslinking of the nanofibers, based on thiol addition to the SBR double bonds, as demonstrated by real-time Infrared spectroscopy analyses. It is proved that by varying the PEO template polymer and the thiol crosslinker content, a fine control of the chemical composition, morphology, water solubility, and thermal properties of the nanofibrous membranes is ensured. Moreover, comparable mechanical properties to those of fibrous membranes produced by conventional electrospinning of organic solvent-based solutions are obtained, clearly showing the attractiveness of the present method, especially in terms of process sustainability.

Handling Editor: Gregory Rutledge.

Address correspondence to E-mail: parnian.kianfar@gmail.com; alessandra.vitale@polito.it

🍃 Springer

GRAPHICAL ABSTRACT

SBR/PEO crosslinked electrospun membrane

SBR crosslinked electrospun membrane
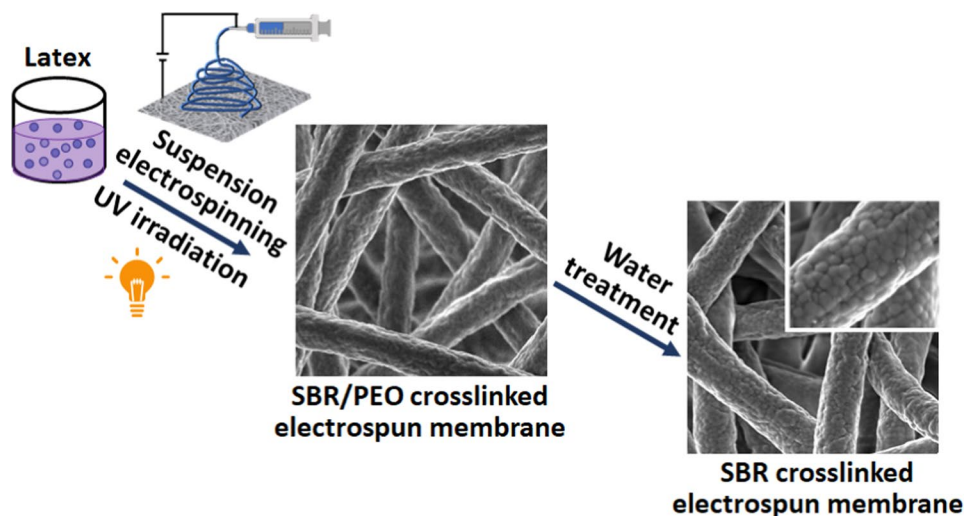
Introduction

Electrospinning is a fascinating and versatile technique that allows to prepare micro- and nanofibers and non-woven fibrous membranes suitable for a broad range of applications, such as textiles, filters, tissue engineering, drug delivery, wound healing, food packaging, sensors, and catalysis, among others [1–7]. One of the main strong points of electrospinning is the possibility to process a large set of polymers, both natural and synthetic. In particular, being polybutadiene-based polymers characterized by high elasticity and extensibility, flexibility, low hysteresis loss, excellent resilience, and high abrasion resistance, rubber electrospun nanomaterials are interesting due to their lightweight, high stretchability, porosity, breathability, and area-to-volume ratio. Accordingly, they can play an important role in the development of high-performance devices, such as stretchable or wearable electronics [8], flexible sensors and actuators [9, 10], selectively permeable membranes and filters [11, 12], as well as energy devices [13]. However, electrospinning of polybutadiene-based polymers has not been extensively studied, and there are only few works in the literature focusing on fiber fabrication of these rubbery materials [14–19]. In fact, such electrospinning process can be challenging: Due to the high viscoelasticity and high molecular weight of the polymers, poor spinning ability and unsteady process are reported.

Moreover, being their glass transition temperature (T_g) below room temperature, such polymers struggle with the tendency to cold flow over time [20, 21]. This is a very well-known drawback in rubber processing and storage, which becomes a serious issue in the case of fibrous structures, as the fibers gradually increase their diameter over time after the electrospinning and eventually collapse together [19]. In order to tackle this issue, chemical crosslinking can be applied to inhibit the movement of the polymer macromolecules and to prevent the overall flowing of the material.

Being rich in C=C double bonds, polybutadiene-based polymers are potential candidates for photo-induced crosslinking reactions. Upon UV irradiation, the allylic hydrogen atoms in the α position of the double bonds can be abstracted [22, 23], and subsequently, the generated radicals can trigger the chemical crosslinking. The photo-crosslinking process of polybutadienes can be made more efficient and substantially accelerated by the addition of multifunctional thiol monomers that copolymerize with C=C double bonds of butadiene, especially with the easily accessible pendant vinyl groups [24]. Generally, thiol-ene polymerization follows a free-radical step-growth addition mechanism, in which propagation and chain-transfer reactions continually cycle [25]. When a diene or a polyene reacts with a multifunctional thiol, a polymer network is formed: Photo-initiated thiol-ene chemistry is thus a highly

efficient way to crosslink polybutadiene-based rubbers in a fast manner [26–28].

It has been previously demonstrated by our group that the coupling of electrospinning and thiol-ene photo-crosslinking of butadiene-based polymers allows fine-tuning the morphology of the nanofibrous mats, in terms of the fiber diameter up to the nanometer range and of the membrane porosity [19]. However, solution electrospinning of polybutadiene-based polymers requires the use of harsh, toxic, and often flammable organic solvents (e.g., tetrahydrofuran, dichloromethane, toluene, dimethylformamide), which raise concerns about environmental and safety issues. Therefore, the development of more sustainable electrospinning processes of polybutadiene-based polymers whose properties are similar to those obtained by solution electrospinning is envisaged. Suspension electrospinning is a novel technology that has emerged in the last years as a smart alternative to overcome the limitations of solution electrospinning [29–35]. Suspension electrospinning consists of electrospinning a stable dispersion of polymer micro-/nanoparticles in water (i.e., a latex). In general, a small quantity of an easily electrospinnable water-soluble polymer (e.g., polyethylene oxide, PEO, or polyvinyl alcohol, PVA), acting as a template, is required and can be subsequently removed [30]. Using this technology, water-insoluble polymers can be electrospun using water as process medium, thus allowing to reduce concerns regarding safety, toxicology, and environmental problems. In addition, higher concentrations than the ones used in solution electrospinning can be processed, enhancing the fibers production rate. For these reasons, suspension electrospinning is often referred as green electrospinning.

Herein, a styrene-butadiene rubber (SBR) latex was processed by suspension electrospinning to fabricate polybutadiene-based nanofibers without using any toxic solvent (water was the only medium for electrospinning). PEO was employed as template polymer, and a multifunctional thiol monomer and appropriate photo-initiators were introduced in the electrospinning suspensions: The electrospun membranes were irradiated at ambient conditions to trigger the photo-induced thiol-ene crosslinking reaction and thus improve their stability. The effect of the composition of the electrospinning suspensions, in terms of thiol crosslinker and PEO template contents, was investigated. The kinetics and the efficiency of the photo-crosslinking, together with the morphological
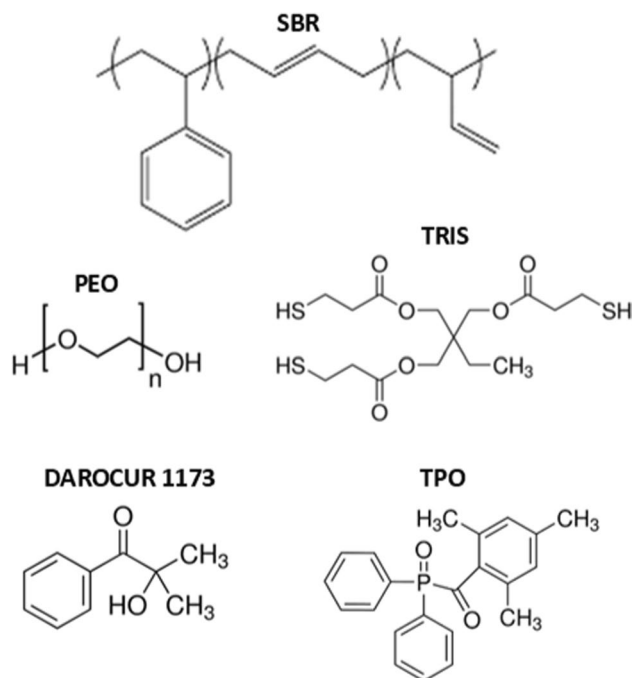

Figure 1 Chemical structure of the materials used to produce photo-crosslinked rubber electrospun membranes, including SBR polymer, PEO template, TRIS thiol crosslinker, TPO, and Darocur 1173 photo-initiators.

and thermal properties of the SBR/PEO fibrous membranes, were studied. Ultimately, PEO could be easily extracted from the nanofiber mats by a simple water treatment procedure, and the photo-crosslinked SBR nanofibrous membranes were characterized.

Experimental section

Materials

The SBR latex Elastolan S19, an aqueous dispersion of a 50 wt% of styrene-butadiene copolymer (100–200 nm particle size, T_g = 6 °C, and viscosity of 200 cP s at 25 °C), was provided by RESCOM srl. Polyethylene oxide (M_w = 1,000,000 g/mol) was purchased from Sigma-Aldrich and used as water-soluble electrospinning template polymer. Trimethylolpropane tris(3-mercaptopropionate) (TRIS) from Bruno Bock was used as thiol crosslinker. Diphenyl (2,4,6-trimethylbenzoyl) phosphine oxide (TPO) and 2-hydroxy-2-methyl-1-phenyl-1-propanone (Darocur 1173) were provided by Ciba Specialty Chemicals and
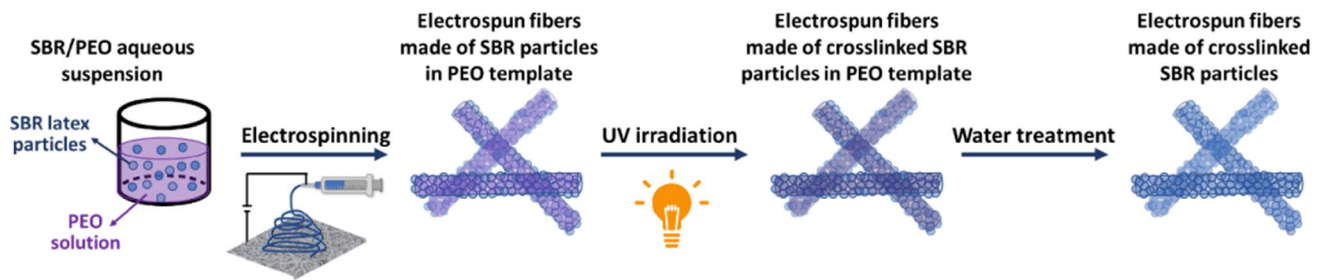
Figure 2 Schematic illustration of SBR fibrous membranes preparation by latex electrospinning and photo-crosslinking. After the SBR particles are dispersed in PEO template aqueous solution, electrospinning and subsequent thiol-ene photo-induced crosslinking are applied. Then, a water treatment is performed to remove the un-cured PEO, leaving crosslinked rubber fibers formed by SBR nanoparticles.

used as photo-initiators. The chemical structures of the employed materials are reported in Fig. 1.

Electrospun mats preparation

The electrospinning suspensions were prepared by mixing the SBR aqueous dispersion and a PEO aqueous solution. Specifically, PEO 5 wt% aqueous solution was prepared through magnet-stirring overnight, then the SBR latex was added, and the suspension was homogenized by magnet-stirring for 2 h. Afterward, the photo-initiating system (TPO/Darocur 1173 1/1 wt/wt) and the TRIS crosslinker were added to the suspension, and a final 15-min magnet-stirring was performed. Different SBR/PEO composition ratios and different TRIS contents were tested: The composition of the prepared suspensions is detailed below. The unit of measure for each component was phr (parts per hundred rubber), considering the SBR polymer as 100 parts.

The viscosity of the investigated electrospinning suspensions was measured using a MCR 702e Multi-Drive Rheometer (Anton Paar) equipped with a parallel-plate configuration, with diameter of 25 mm. The shear viscosity was measured at a shear rate of $10 \, \text{s}^{-1}$ at 25 °C and setting 0.5 mm as the gap between the upper plate and the platform.

Electrospinning was performed by an E-fiber electrospinning system SKE apparatus in horizontal setup with a plane stationary collector, using an aluminum foil as substrate. A syringe tip diameter of 1 mm was employed, the feed rate was set at 0.2–0.3 ml/h, the working distance at 15 cm, and a voltage of 13–17 kV was applied. Throughout the electrospinning process, the temperature and relative humidity were 25 °C and 45%, respectively.

Immediately after electrospinning, the samples were irradiated by UV light using a high-pressure mercury-xenon lamp equipped with an optical fiber LIGHTNINGCURE Spotlight source LC8, Hamamatsu. The irradiation was performed in air condition with a light intensity of $32 \, \text{mW/cm}^2$ for 5 min. The UV light intensity was measured using a UV Power Puck® II from EIT® Instrument Markets.

After electrospinning and UV irradiation, in order to remove the PEO polymer, samples were immersed in distilled water for 24 h and then dried in oven at 60 °C for 3 h.

At the end of the fabrication process, flexible free-standing fibrous mats having thickness of 30–50 μm were obtained. The thickness was measured by digital micrometer; for each sample, at least five values in different spots of the membrane were collected, and the average value was calculated.

The schematic representation of the whole process to obtain fibrous materials made of crosslinked SBR particles is depicted in Fig. 2.

Electrospun mats characterizations

The chemical structure of the samples prior and after UV irradiation was analyzed by Fourier Transform Infrared (FTIR) spectroscopy by using a Thermo Fisher Scientific Nicolet™ iS50 spectrometer in the spectral range of $4000–400 \, \text{cm}^{-1}$. The spectra were collected both in transmission mode and in attenuated total reflectance (ATR) mode with an accumulation of 32 scans at a resolution of $4 \, \text{cm}^{-1}$. Moreover, real-time FTIR analyses were carried out: Simultaneously, with

the FTIR scan acquisition in transmission mode, electrospun mats were irradiated. The spectra were collected with one spectra/scan at a resolution of 4 cm^{-1}, by using a liquid nitrogen-cooled mercury–cadmium–telluride (MCT) detector. UV irradiation was applied with an intensity of 32 mW/cm^2, by a high-pressure mercury-xenon lamp equipped with an optical fiber LIGHTNINGCURE Spotlight source LC8 (Hamamatsu). Silicon wafers were used as transparent substrates to IR wavelengths, and measurements were taken in ambient condition. Upon UV irradiation, crosslinking conversion was followed by monitoring the decrease in the C=C double bonds of the SBR (vinyl and *trans*-butene, at 910 cm^{-1} and 962 cm^{-1}, respectively) and of the SH thiol groups of the crosslinker (at 2565 cm^{-1}) as a function of the irradiation time t [24]. The absorption band area of the reactive groups A was normalized by the area of the peak at 699 cm^{-1}, related to out-of-plane bending of the CH groups in the aromatic ring, A_{ref}, used as reference. Functional groups conversion is calculated by Eq. 1:

$$\text{Conversion (\%)} = \left(1 - \frac{|A/A_{ref}|_t}{|A/A_{ref}|_{t=0}} \right) \times 100 \qquad (1)$$

The peak areas were quantified through the Omnic™ software. Three replicas were averaged, and the error was calculated.

The insoluble fraction of the photo-cured electrospun mats was measured gravimetrically by calculating the mass loss after 24-h extraction in water and 3h drying at 60 °C.

The morphology of the fibrous mats was analyzed using a Merlin field emission scanning electron microscopy (FE-SEM), ZEISS. Prior to FE-SEM imaging, samples were sputter coated with ~ 10 nm Cr film using a Quorum Q150T ES sputter coater. The distribution of fiber diameters was obtained by ImageJ software analyzing the FE-SEM images: Approximately 100 measurements were taken for each sample.

Thermal stability and resistance were characterized by thermogravimetric analysis (TGA) using a Mettler Toledo TGA/SDTA 851^e apparatus. TGA was carried out in the temperature range 25–800 °C with a heating rate of 10 °C/min and a constant nitrogen flux of 60 ml/min in order to avoid thermo-oxidative processes.

Thermal properties including the glass transition temperature, the enthalpy of melting (ΔH_m), and the melting point (T_m) were measured through differential scanning calorimetry (DSC) experiments using a DSC1 STARe Mettler Toledo instrument. DSC was carried out in a heating–cooling–heating cycle from − 60 °C to 180 °C, with a heating and cooling rate of 20 °C/min and a constant nitrogen flux of 60 ml/min. T_g was obtained from the midpoint of the heat increment in the second heating cycle, and T_m was obtained from the maximum of the endothermic peak in the second heating cycle. For PEO-containing samples, the crystallinity degree X_c was measured by calculating ΔH_m in the second heating cycle, with respect to the enthalpy of melting for a 100% crystalline PEO sample ($\Delta H_{m,0} = 196$ J/g [36]) at the equilibrium melting point ($T_{m,0}$).

The viscoelastic properties of the electrospun samples were analyzed through dynamic mechanical thermal analysis (DMTA) using a Triton Technology instrument. Analyses were performed in tensile configuration, in a temperature range from − 100 to 100 °C, with a heating rate of 3 °C/min and a frequency of 1 Hz on samples with approximate dimensions of 20 mm × 10 mm × 50 μm.

Tensile mechanical properties were evaluated using an INSTRON 3366 electromechanical universal testing machine (ITW Test and Measurement Italia S.r.l., Instron CEAST Division) equipped with a 500-N load cell. Samples with approximate dimensions of 30 mm × 8 mm × 50 μm were used. Measurements were taken in ambient conditions by applying a constant stretching speed of 5 mm/min. During the tensile testing, the stress (through machine-recorded force) and strain (the displacement based on initial cross-section area and gauge length) were measured. At least five replicates were tested. The Young's modulus E (evaluated in the initial linear elasticity regime of the stress–strain, which corresponds to a strain in the range 0.05–0.1 mm/mm), the elongation at break, and the UTS (ultimate tensile strength) of the samples were calculated.

Results and discussion

Fibrous membranes preparation by latex electrospinning and photo-crosslinking

The addition of PEO in the electrospinning suspension was necessary as the SBR latex was found to be non-electrospinnable by its own (i.e., a stable jet could not be formed). Whereas, with the addition of a small amount of PEO, as low as 7.5 phr, latex

Table 1 Composition of the latex-based formulations used for electrospinning

| Sample name	PEO (phr)	Photo-initiator (phr)	TRIS (phr)	Solid content (wt%)	Viscosity (cPa s)
SBR/30PEO/3TRIS	30	1	3	16.2	n/a
SBR/30PEO/10TRIS	30	1	10	16.0	740
SBR/30PEO/50TRIS	30	1	50	15.2	180
SBR/15PEO/10TRIS	15	1	10	22.5	n/a
SBR/7.5PEO/10TRIS	7.5	1	10	29.8	590
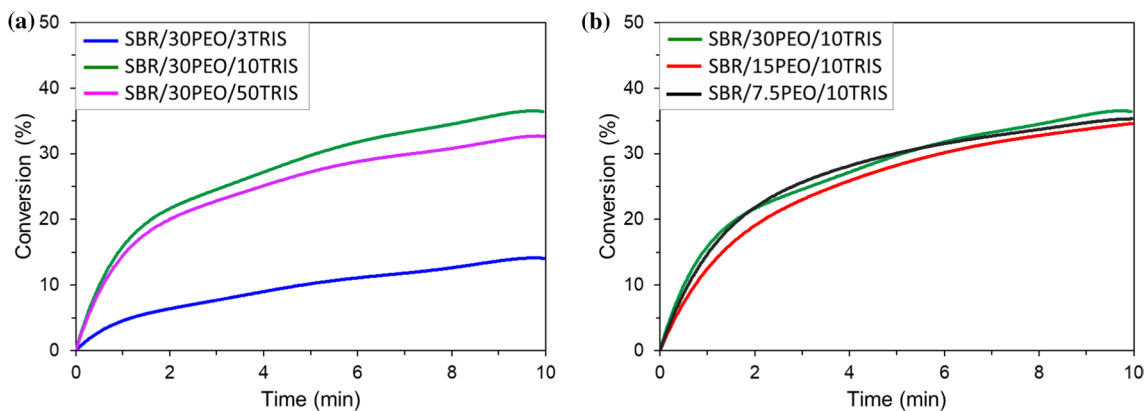
Figure 3 Photo-induced crosslinking kinetics by real-time FTIR spectroscopy: vinyl C=C conversion as a function of UV irradiation time for electrospun mats made from different SBR/PEO/ TRIS formulations. **a** Effect of thiol crosslinker TRIS content and **b** effect of template polymer PEO content.

electrospinning process was stable. The electrospinning of SBR/PEO suspensions thus resulted in the successful fabrication of nanofibrous membranes made of uniform and continuous fibers composed of both SBR and PEO (Fig. S1 of the Supplementary Information). However, being un-crosslinked, the fibers tended to form connection points and to collapse upon few days of storage, due to the cold flow of the rubber polymer [19]. Photo-crosslinking of SBR, in the presence of a suitable photo-initiating system and a multifunctional thiol crosslinker (TRIS) reacting with the double bonds, was therefore applied to stabilize the fibrous structure. The amount of the photo-initiator was fixed at 1 phr with respect to SBR content, while different amounts of crosslinker were evaluated (i.e., 3, 10, and 50 phr), maintaining a fixed SBR/PEO ratio, corresponding to 100/30 wt/wt. Moreover, at a fixed SBR/TRIS ratio of 100/10 wt/wt, the influence of PEO content on the electrospinning process and on the properties of the fibrous mats was also examined, changing the quantity of PEO in the range 7.5–30 phr. The details of the investigated formulations together

with their names, their viscosities, and the indication of the total solid content are reported in Table 1.

In order to study the kinetics of the photo-induced thiol-ene crosslinking reaction, real-time transmission FTIR spectroscopy was conducted on the SBR/ PEO electrospun fibers. Figure 3a shows the effect of the thiol crosslinker amount on the crosslinking kinetics, displaying the conversion of the SBR pendant vinyl (at 910 cm^{-1}) as a function of irradiation time. The systems containing 10 and 50 phr of TRIS had a similar conversion curve, reaching a comparable double bond conversion of 36 ± 4% and 33 ± 4%, respectively, after 10 min of irradiation. This result suggests that the SBR/TRIS 100/10 wt/ wt ratio supplied enough thiol moieties for an efficient copolymerization of the vinyl groups. In the SBR/30PEO/50TRIS formulation, there was instead an excess of thiol crosslinker, without any change in the reaction rate. Whereas, the system with 3 phr of TRIS showed a much lower conversion: Only a value of 14% was obtained after 10 min of irradiation. In this case, the thiol groups concentration was
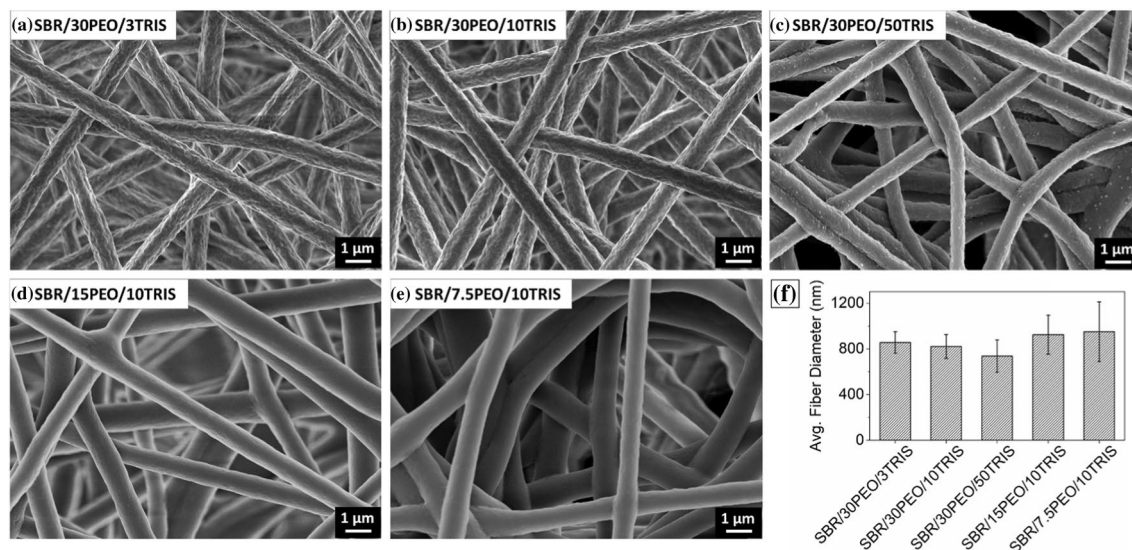
Figure 4 Morphology of the photo-crosslinked electrospun membranes fabricated from SBR/PEO/TRIS aqueous suspensions. **a–e**: FE-SEM images of SBR/30PEO/3TRIS (**a**), SBR/30PEO/10TRIS (**b**), SBR/30PEO/50TRIS (**c**), SBR/15PEO/10TRIS (**d**), and SBR/7.5PEO/10TRIS (**e**) membranes. **f**: Average fiber diameter of the mats.

much lower than that of the vinyl unsaturations: After their rapid consumption, the thiol monomer was rapidly consumed, and then the conversion of the vinyl double bonds continued slowly mainly due to homopolymerization.

Figure 3b shows the vinyl conversion curves for samples with a different content of PEO. As expected, as PEO does not take part in the thiol-ene crosslinking, its content did not affect the reaction kinetics.

It is well-known that the pendant vinyl groups are much more reactive toward thiyl radicals (RS·) than the backbone 2-butene double bonds of the butadiene chains [27, 37]. Accordingly, for SBR/30PEO/3TRIS, SBR/30PEO/10TRIS and SBR/30PEO/50TRIS systems, the conversion of the 2-butene C=C bonds (at 962 cm^{-1}) was found to be much lower than the vinyl groups conversion (Fig. S2 of the Supplementary Information).

Moreover, the SH group consumption could be tracked in the FTIR spectra of the system containing the highest amount of TRIS, meaning SBR/30PEO/50TRIS. Interestingly, the thiol conversion was found to be very similar to the vinyl conversion (~ 32% after 10 min of irradiation, as shown in Fig. S3 of the Supplementary Information). The reason for this low thiol conversion may lay in the lack of enough accessible neighboring double bonds. Moreover, the fibrous morphology, the particle shape of SBR, and the solid state can restrict the molecules movement and further reduce the number of accessible C=C groups.

Characterization of the photo-crosslinked SBR/PEO electrospun membranes

The fibrous morphology of the photo-cured electrospun mats was analyzed by FE-SEM analyses: Results are shown in Fig. 4. Interestingly, the photo-crosslinked SBR/PEO fibers have uniform cylindrical shape, well-defined borders along their length and did not exhibit any collapsing point. The photo-induced thiol-ene reaction was thus demonstrated to make the rubber fibers shape-stable: The SBR flowing, which is responsible for the fiber collapsing, is inhibited, and the fibrous morphology remains unchanged over time. The investigated systems show good-quality fibers with diameter in the range ~ 735–970 nm (Fig. 4f), with a quite narrow size distribution (the fiber diameter distributions for the different systems are shown in Fig. S4 of the Supplementary Information).

The morphology of the nanofibrous membranes was found to be affected by both the viscosity and the solid content of the electrospinning formulation, which are indeed dependent on its composition. By increasing the TRIS crosslinker content, the average fiber diameter slightly decreases, mainly due to the

Table 2 Comparison between the theoretical amount of PEO and the water-soluble fraction of the photo-crosslinked electrospun mats made from formulations with different TRIS and PEO contents

Sample	Theoretical PEO content (wt%)*	Water-soluble fraction (wt%)
SBR/30PEO/3TRIS	22.4	19.4
SBR/30PEO/10TRIS	21.3	18.7
SBR/30PEO/50TRIS	16.6	19.5
SBR/15PEO/10TRIS	11.9	11.1
SBR/7.5PEO/10TRIS	6.3	5.9

*Theoretical PEO content is obtained based on initial suspension formulations for electrospinning

lower viscosity of the formulation (Table 1). Moreover, it seems that the lower the TRIS content, the coarser the surface of the electrospun fibers. Whereas, by increasing the PEO content, the average fibers diameter is decreased, together with the width of their size distribution, although the viscosity slightly increases (Table 1). This means that in this case the solid content, which increases with the SBR/PEO ratio (Table 1), is the predominant factor governing the fibers size. Finally, as PEO template is easily and successfully electrospinnable, the higher its concentration, the better the fiber-forming process, and the thinner and more uniform the fibers.

To better investigate the chemical composition of the nanofibers, their water solubility was tested, considering that PEO is soluble in water, while SBR is not. As reported in Table 2, the quantity of PEO in the fibers was approximately equal to that of the initial formulations, meaning that the electrospinning process does not modify the SBR/PEO ratio of the samples. Moreover, the fact that PEO remained soluble in water after UV irradiation of the fibrous mats suggests that

the photo-crosslinking thiol-ene reaction of SBR and TRIS is much favored (and faster) with respect to the photo-induced crosslinking of PEO [38].

For the SBR/30PEO/50TRIS sample, the water-soluble fraction of the nanofibers was slightly higher than the amount of PEO (Table 2). This is probably due to the solubilization of the excess of thiol crosslinker.

The thermal properties of the samples were studied: The DSC scans of all the investigated SBR/PEO photo-crosslinked electrospun mats (Fig. 5a) showed a T_g in the range 7–12 °C, which could be associated to the SBR component of the nanofibers, and a T_m in the range 61–66 °C, due to the melting of PEO moieties (Table 3). Both the T_g and the T_m were not significantly affected by the fibers composition and by the photo-crosslinking reaction. Only the SBR/30PEO/50TRIS system showed a reduced melting point and a reduced glass transition temperature (Table 3), probably due to the fact that the un-cured low-molecular-weight crosslinker can act as plasticizer. By calculating the ΔH_m from the second heating cycle of the DSC scans,

Table 3 Thermal properties of the photo-crosslinked SBR/PEO electrospun membranes and of pristine SBR and PEO cast films

Sample	T_g (°C)	T_m (°C)	X_c (%)	T_{10} (°C)
SBR	11	–	–	369
PEO	<-20	72	63.3	375
SBR/30PEO/3TRIS	12	65	11.8	365
SBR/30PEO/10TRIS	11	66	11.1	359
SBR/30PEO/50TRIS	7	61	10.1	326
SBR/15PEO/10TRIS	11	65	2.8	367
SBR/7.5PEO/10TRIS	11	61	0.6	362

Glass transition temperature T_g, melting temperature T_m, and crystallinity degree X_c from DSC analyses, and T_{10} (temperature at which 10% of the initial weight is lost) from TGA analyses

Figure 5 Thermal analyses of the photo-crosslinked electrospun membranes, in addition to those of pristine SBR and PEO cast films. **a**: DSC scans of the second heating cycle and **b**: TGA thermograms.
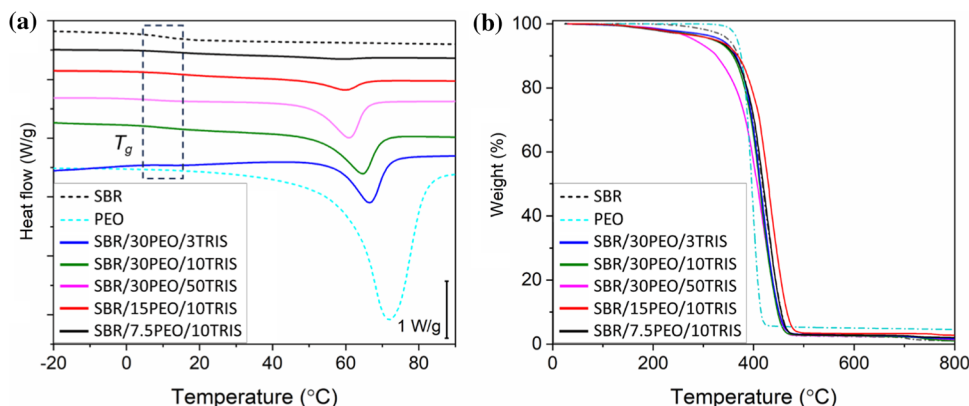
Figure 6 Morphology of the photo-crosslinked electrospun membranes after water treatment (WT) for PEO removal. **a–d**: FE-SEM images of SBR/30PEO/3TRIS-WT (**a**), SBR/30PEO/10TRIS-WT (**b**), SBR/15PEO/10TRIS-WT (**c**), and SBR/7.5PEO/10TRIS-WT (**d**) samples. The insets of **a** and **b** are the same sample with higher magnification for better showing the SBR nanoparticles. **e**: Average fiber diameter of the mats after PEO removal.
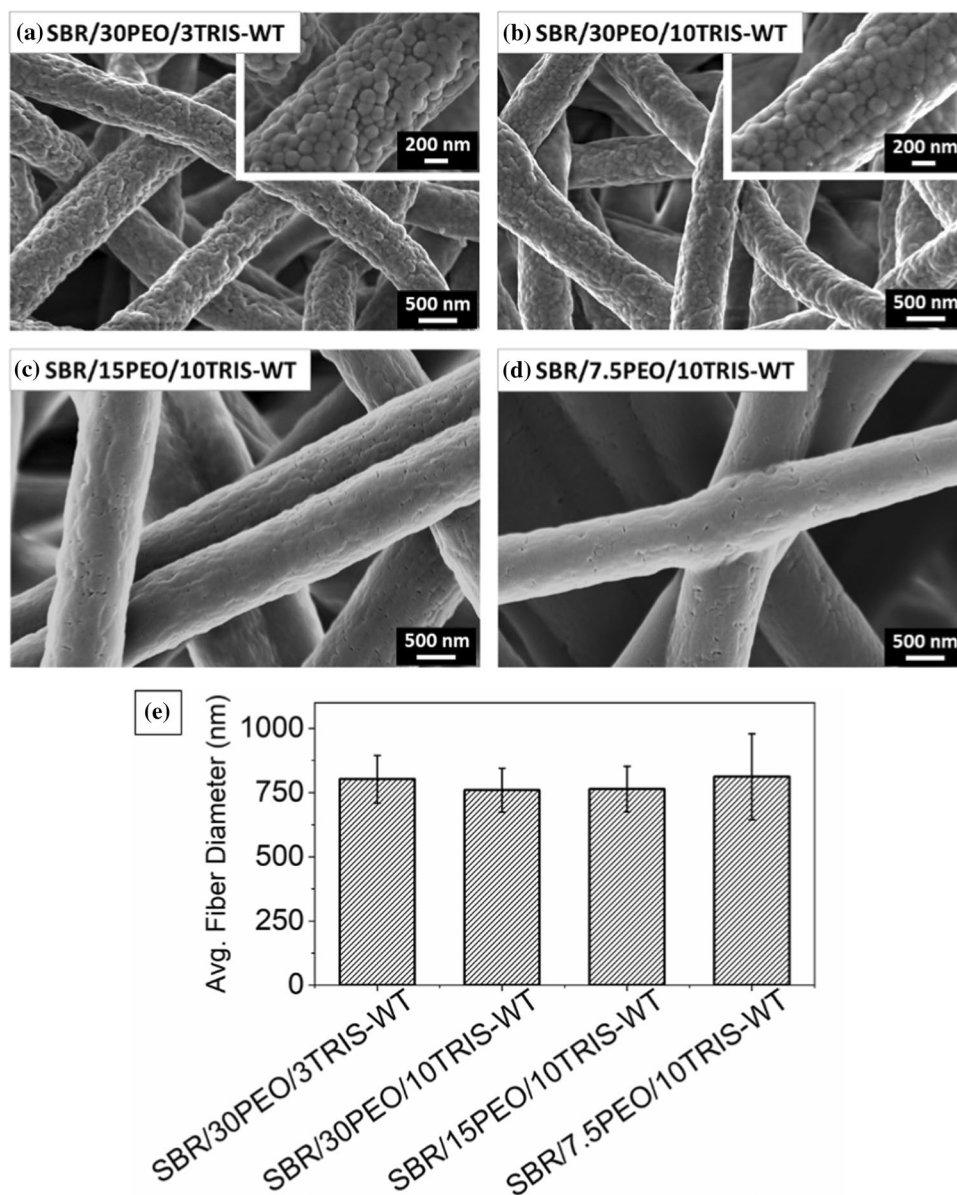
the crystallinity degree of the samples could be estimated (Table 3). Indeed, X_c is proportionally related to the content of PEO polymer in the fibrous structure.

The thermal resistance of the SBR/PEO electrospun photo-crosslinked mats was evaluated by TGA analyses (Fig. 5b). All samples exhibited excellent resistance, with a T_{10} (i.e., the temperature at which 10% of the initial weight of the sample is lost) > 360 °C, except the formulation containing 50-phr TRIS (SBR/30PEO/50TRIS), which underwent its major weight loss starting from 320 °C. This is probably due to the degradation of the residual un-reacted thiol crosslinker. Because of its inferior thermal properties,

this sample (i.e., SBR/30PEO/50TRIS) was not subjected to further characterizations.

Characterization of the photo-crosslinked SBR electrospun membranes after PEO removal

As discussed above, the template polymer PEO could be easily removed by a water treatment (WT), allowing to obtain fibrous membranes fully made of SBR. The morphology of the fibrous mats after PEO removal was analyzed by FE-SEM imaging, as shown in Fig. 6 and in Fig. S5 of the Supplementary Information. Even after the water treatment, the photo-crosslinked

SBR membranes showed uniform and regular fibers, thus demonstrating that the photo-induced reaction assures the shape-stability of the systems. While the fibers surface prior to PEO removal was smooth and the SBR particles could not be detected (Fig. 4), the water treatment step resulted in a higher surface roughness and porosity of the fibers. The samples with the highest PEO content (i.e., SBR/30PEO/3TRIS and SBR/30PEO/10TRIS) displayed a particular surface nanostructure with high surface area, reminding a raspberry, being the fibers composed of distinct rubber particles partially fused together (Fig. 6a and b). The removal of the PEO template thus made visible the individual photo-crosslinked SBR particles, also demonstrating that such particles are able to maintain their shape for a long time. The rubber particle diameter was 105 ± 4 nm, similar in the two samples and comparable to the size of the SBR particles in the starting latex, hence confirming their efficient stabilization by photo-crosslinking.

Instead, the samples with a lower content of PEO (i.e., SBR/15PEO/10TRIS and SBR/7.5PEO/10TRIS) exhibited fibers with a rough surface made of collapsed rubber particles, which were not individually detectable (Fig. 6c and d). This can be due to the presence of more contact points among the rubber particles during the photo-crosslinking reaction: The lower amount of PEO chains surrounding the particles could not keep them apart, leading to their tendency to adhere together forming a cohesive structure. Moreover, some small holes are clearly visible on the fibers, as a result of the removal of the template polymer. The morphology of the rubber nanofibrous membranes can thus be tuned by changing both the composition of the electrospinning suspension and the fabrication process (e.g., application of a water treatment).

The average diameter of the fibers decreased after water treatment (Fig. 6e): Values in the range 757–811 nm were found. This is clearly due to the PEO removal from the electrospun fibers.

In order to evaluate the chemical composition of the nanofibers, FTIR spectra of photo-crosslinked electrospun membranes prior and after water treatment were collected and compared. As an example, Fig. 7 shows the results for SBR/30PEO/10TRIS system: after water treatment, the characteristic absorption peaks of PEO (centered at 843 cm^{-1} and 1090 cm^{-1} and associated to ether groups) had a much lower intensity, even though were still present. Therefore, these results suggest that although most
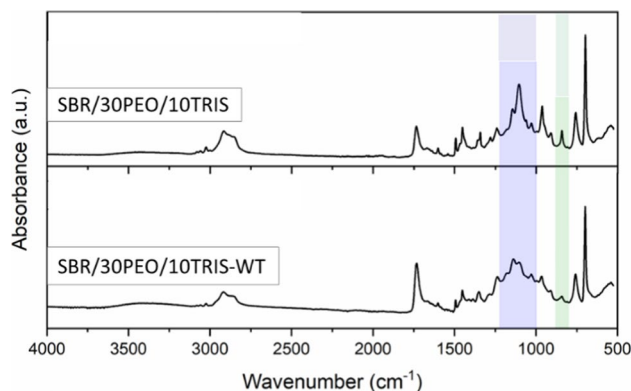
Figure 7 FTIR spectra of SBR/30PEO/10TRIS photo-crosslinked electrospun sample before and after water treatment (WT) for PEO removal.

Table 4 Thermal properties of the photo-crosslinked SBR-based electrospun membranes

Sample	T_g (°C)	T_m (°C)	X_c (%)	T_{10} (°C)
SBR/30PEO/3TRIS-WT	10	59	5.2	375
SBR/30PEO/10TRIS-WT	10	60	4.5	374
SBR/15PEO/10TRIS-WT	11	57	1.9	374
SBR/7.5PEO/10TRIS-WT	11	53	0.5	367

Glass transition temperature T_g, melting temperature T_m, and crystallinity degree X_c from DSC analyses, and T_{10} (temperature at which 10% of the initial weight is lost) from TGA analyses

of PEO component was removed from the nanofibers (see solubility results in Table 2), some traces were still present, proportionally to the initial amount of PEO in the electrospinning formulation. In fact, it is possible that some PEO chains remained trapped in the crosslinked rubber network, and also that a partial PEO photo-induced crosslinking reaction took place during UV irradiation.

DSC analyses (results are reported in Fig. S6 of the Supplementary Information and in Table 4) did not show any significant change before and after water treatment in the values of T_g related to the rubber component. Instead, crystallinity was lower than in SBR/PEO electrospun mats, with X_c proportional to the remaining PEO content after water treatment. Interestingly, also the T_m was found to be lower after PEO removal: This means that the remaining PEO chains could rearrange differently during the water treatment. Moreover, a lower amount of residual PEO resulted into a lower T_m (Table 4).

Figure 8 Mechanical properties of SBR/30PEO/10TRIS photo-crosslinked electrospun membranes prior and after water treatment (WT) for PEO removal: DMTA results (**a**) and an example of tensile stress–strain curves (**b**).
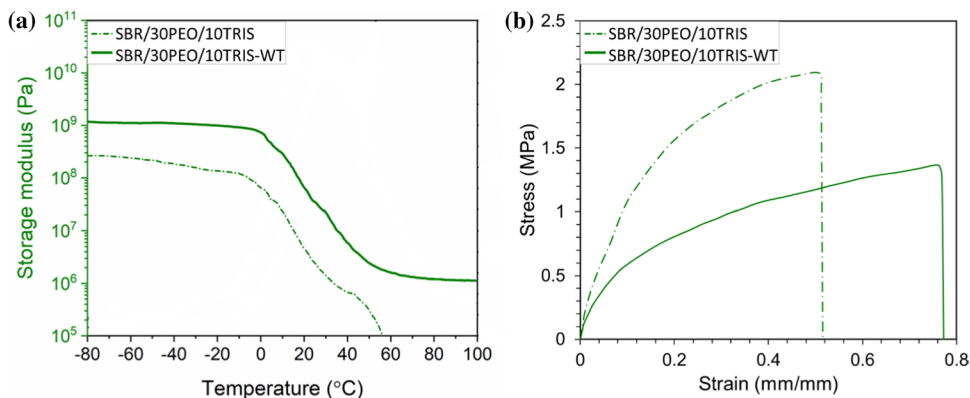
After water treatment, as shown in Fig. S6 of the Supplementary Information and in Table 4, the electrospun mats presented a slightly better thermal resistance: T_{10} values (Table 4) are higher, probably due to the removal of un-reacted monomer during the water treatment step.

Finally, the viscoelastic properties of the photo-crosslinked electrospun membranes were examined through DMTA experiments. As an example, Fig. 8a shows the storage modulus of the SBR/30PEO/10TRIS fibrous mats before and after PEO removal. SBR/PEO membranes before water treatment showed a severe drop of storage modulus around the melting point of PEO (~ 60 °C), due to the polymer flowing. While, after PEO removal, the fibrous samples exhibited the typical trend of a crosslinked network, as the storage modulus reached a plateau in the rubbery regime. These results confirm that the thiol-ene photo-curing reaction allows to form an adequately crosslinked network within the fibers, and that the PEO component is efficiently removed by the water treatment.

Considering that the final rubber fibers obtained from latex electrospinning and subsequent PEO removal are composed of SBR particles and can have a special raspberry-like morphology, their mechanical properties could differ from those of SBR electrospun fibers with a homogenous structure obtained by solution electrospinning and photo-crosslinking [19]. Tensile tests were thus performed on SBR/30PEO/10TRIS mats before and after PEO removal. Figure 8b shows an example of collected stress–strain curves for these samples (other curves are shown in Fig. S7 of the Supplementary Information): An elastic modulus E of 18.4 ± 3.2 MPa and 13.1 ± 4.8 MPa, an elongation at break of $51 \pm 9\%$ and $75 \pm 12\%$, and an UTS of 2.0 ± 0.4 MPa and 1.4 ± 0.2 MPa were obtained before and after PEO removal, respectively. The presence of PEO in fact increases E and UTS but decreases the stretchability of the rubber nanostructured mats.

Interestingly, although their morphology is different, the fibrous SBR membranes from latex electrospinning exhibited comparable mechanical strength to the membranes produced by solution electrospinning coupled with photo-crosslinking [19], while their extensibility is slightly lower. These results suggest that in the investigated fibers from suspension electrospinning, the photo-induced crosslinking of the SBR occurs not only within each spherical rubber particle but also among different adjacent particles.

Conclusions

The work proposed a sustainable approach to prepare ultrafine shape-stable rubber fibrous membranes based on the electrospinning of a SBR latex coupled with thiol-ene photo-induced crosslinking in ambient conditions, using water as the only medium during the whole process. By varying the amount of the template polymer PEO and the concentration of the thiol crosslinker, thus changing the viscosity and the solid content, the electrospun membranes showed tunable fiber size and morphology. Fibrous membranes made of SBR and PEO exhibited a uniform morphology, good thermal resistance (degradation started at $T > 360$ °C), but instability above PEO melting point (~ 60 °C). Whereas, when PEO was removed by water extraction, raspberry-like nanofibers, namely formed by the assembly of distinct round rubber nanoparticles with a diameter of ~ 105 nm, only partially fused together, could be obtained. The photo-crosslinked rubber electrospun mats showed good stability,

excellent thermal resistance (degradation started at $T > 370\ °C$) and mechanical resistance, and stretchability similar to those of their homologues obtained by solution electrospinning.

This work thus demonstrates that suspension electrospinning is a green, attractive, and versatile technology to fabricate rubber nanofibrous membranes with tunable chemical composition, morphology, water solubility, and thermal properties, which can be promising materials for different applications, especially those requiring flexibility and stretchability.

Acknowledgements

Author contributions

PK was involved in investigation, writing—original draft, writing—review and editing, and visualization; AB participated in investigation; SDV helped in investigation and writing—review and editing; RB was involved in conceptualization and writing—review and editing; and AV participated in conceptualization, writing—review and editing, visualization, and supervision.

Funding

Data availability

The data that support the findings of this study are available from the corresponding author upon request.

Declarations

Conflict of interest The authors declare that they have no known competing financial interests or personal relationships that could have appeared to influence the work reported in this paper.

References

[1] Xue J, Wu T, Dai Y, Xia Y (2019) Electrospinning and electrospun nanofibers: methods, materials, and applications. Chem Rev 119(8):5298–5415

[2] Li Y, Zhu J, Cheng H, Li G, Cho H, Jiang M et al (2021) Developments of advanced electrospinning techniques: a critical review. Adv Mater Technol 6(11):2100410–2100438

[3] Shi S, Si Y, Han Y, Wu T, Iqbal MI, Fei B et al (2022) Recent progress in protective membranes fabricated via electrospinning: advanced materials, biomimetic structures, and functional applications. Adv Mater 34(17):2107938–2107968

[4] Zhou Y, Liu Y, Zhang M, Feng Z, Yu D-G, Wang K (2022) Electrospun nanofiber membranes for air filtration: a review. Nanomaterials 12(7):1077–1109

[5] Rahmati M, Mills DK, Urbanska AM, Saeb MR, Venugopal JR, Ramakrishna S et al (2021) Electrospinning for tissue engineering applications. Prog Mater Sci 117:100721–100759

[6] Luraghi A, Peri F, Moroni L (2021) Electrospinning for drug delivery applications: a review. J Control Release 334:463–484

[7] Zhao L, Duan G, Zhang G, Yang H, He S, Jiang S (2020) Electrospun functional materials toward food packaging applications: a review. Nanomaterials 10(1):150–181

[8] Xu Q, Liu H, Zhong X, Jiang B, Ma Z (2020) Permeable weldable elastic fiber conductors for wearable electronics. ACS Appl Mater Interfaces 12(32):36609–36619

[9] Wang X, Meng S, Tebyetekerwa M, Weng W, Pionteck J, Sun B et al (2017) Nanostructured polyaniline/poly (styrene-butadiene-styrene) composite fiber for use as highly sensitive and flexible ammonia sensor. Synth Met 233:86–93

[10] Teixeira J, Horta-Romarís L, Abad M-J, Costa P, Lanceros-Méndez S (2018) Piezoresistive response of extruded polyaniline/(styrene-butadiene-styrene) polymer blends for force and deformation sensors. Mater Des 141:1–8

[11] Duong HC, Chuai D, Woo YC, Shon HK, Nghiem LD, Sencadas V (2018) A novel electrospun, hydrophobic, and elastomeric styrene-butadiene-styrene membrane for membrane distillation applications. J Memb Sci 549:420–427

[12] Beshkar F, Salavati-Niasari M, Amiri O (2020) Superhydrophobic–superoleophilic copper–graphite/styrene-butadiene-styrene based cotton filter for efficient separation of oil derivatives from aqueous mixtures. Cellulose 27(8):4691–4705

[13] Isozumi H, Horiba T, Kubota K, Hida K, Matsuyama T, Yasuno S et al (2020) Application of modified styrene-butadiene-rubber-based latex binder to high-voltage operating LiCoO2 composite electrodes for lithium-ion batteries. J Power Sources 468:228332–228341

[14] Fong H, Reneker DH (1999) Elastomeric nanofibers of styrene–butadiene–styrene triblock copolymer. J Polym Sci Part B Polym Phys 37(24):3488–3493

[15] Hao X, Zhang X (2007) Syndiotactic 1, 2-polybutadiene fibers produced by electrospinning. Mater Lett 61(6):1319–1322

[16] Kerr-Phillips TE, Woehling V, Agniel R, Nguyen GTM, Vidal F, Kilmartin P et al (2015) Electrospun rubber fibre mats with electrochemically controllable pore sizes. J Mater Chem B 3(20):4249–4258

[17] Zhang X, Chase GG (2016) Electrospun elastic acrylonitrile butadiene copolymer fibers. Polymer (Guildf) 97:440–448

[18] Kianfar P, Nguyen Trieu HQ, DalleVacche S, Tsantilis L, Bongiovanni R, Vitale A (2022) Solvent-free electrospinning of liquid polybutadienes and their in-situ photocuring. Eur Polym J 177:111453–111462

[19] Vitale A, Massaglia G, Chiodoni A, Bongiovanni R, Pirri CF, Quaglio M (2019) Tuning porosity and functionality of electrospun rubber nanofiber mats by photo-crosslinking. ACS Appl Mater Interfaces 11(27):24544–24551

[20] Wang X, Nie H, Liu D, He A (2017) Retardation of cold flow in immiscible rubber blends by tailoring their microstructures. Polym Int 66(11):1473–1479

[21] Valentini L, Lopez-Manchado MA (2020) Classification of rubbers and components for harsh environmental systems. High-performance elastomeric materials reinforced by nano-carbons. Elsevier, The Netherland, pp 1–14

[22] Bussière PO, Gardette JL, Lacoste J, Baba M (2005) Characterization of photodegradation of polybutadiene and polyisoprene: chronology of crosslinking and chain-scission. Polym Degrad Stab 88(2):182–188

[23] Kagiya VT, Takemoto K (1976) Crosslinking and oxidation of 1, 2-polybutadiene by UV irradiation. J Macromol Sci Part A-Chem 10(5):795–810

[24] Decker C, Viet TNT (1999) Photocrosslinking of functionalized rubbers, 8. The thiol-polybutadiene system. Macromol Chem Phys 200(8):1965–1974

[25] Hoyle CE, Bowman CN (2010) Thiol-ene click chemistry. Angew Chemie-Int Ed 49(9):1540–1573

[26] Ten Brummelhuis N, Diehl C, Schlaad H (2008) Thiol-ene modification of 1, 2-polybutadiene using UV light or sunlight. Macromolecules 41(24):9946–9947

[27] Decker C, Nguyen Thi Viet T (2000) High-speed photocrosslinking of thermoplastic styrene-butadiene elastomers. J Appl Polym Sci 77(9):1902–12

[28] Decker C, Viet TNT (1999) Photocrosslinking of functionalized rubbers, 7 styrene-butadiene block copolymers. Macromol Chem Phys 200(2):358–367

[29] Agarwal S, Greiner A (2011) On the way to clean and safe electrospinning-green electrospinning: emulsion and suspension electrospinning. Polym Adv Technol 22(3):372–378

[30] Stoiljkovic A, Ishaque M, Justus U, Hamel L, Klimov E, Heckmann W et al (2007) Preparation of water-stable submicron fibers from aqueous latex dispersion of water-insoluble polymers by electrospinning. Polymer (Guildf) 48(14):3974–3981

[31] Crespy D, Friedemann K, Popa A (2012) Colloid-electrospinning: fabrication of multicompartment nanofibers by the electrospinning of organic or/and inorganic dispersions and emulsions. Macromol Rapid Commun 33(23):1978–1995

[32] Cacciotti I, House JN, Mazzuca C, Valentini M, Madau F, Palleschi A et al (2015) Neat and GNPs loaded natural rubber fibers by electrospinning: manufacturing and characterization. Mater Des 88:1109–1118

[33] Gonzalez E, Barquero A, Muñoz-Sanchez B, Paulis M, Leiza JR (2021) Green electrospinning of polymer latexes: a systematic study of the effect of latex properties on fiber morphology. Nanomaterials 11(3):706–718

[34] Osei LB, Ndur SA, Fosu S (2022) Synthesis and characterisation of electrospun natural rubber latex/polyvinyl alcohol for application in aqueous processes. J Rubber Res 25(4):313–320

[35] González E, Barquero A, Paulis M, Leiza JR (2023) Fabrication of multifunctional composite nanofibers by green electrospinning. Macromol Mater Eng. 308:2300011–2300020

[36] Zardalidis G, Mars J, Allgaier J, Mezger M, Richter D, Floudas G (2016) Influence of chain topology on polymer crystallization: poly(ethylene oxide)(PEO) rings versus linear chains. Soft Matter 12(39):8124–8134

[37] Decker C, Viet TNT (2000) Photocrosslinking of functionalized rubbers IX Thiol-ene polymerization of styrene-butadiene-block-copolymers. Polymer (Guildf) 41(11):3905–3912

[38] Doytcheva M, Dotcheva D, Stamenova R, Orahovats A, Tsvetanov C, Leder J (1997) Ultraviolet-induced crosslinking of solid poly(ethylene oxide). J Appl Polym Sci 64(12):2299–2307